Journal of Design Against Fatigue

https://minerva-aset.com/JDAF

MINERVA ASET

Application of data mining techniques for assessment of fracture load and energy in double cantilever beam solder joints

Hossein Soroush, Amir Nourani*

Department of Mechanical Engineering, Sharif University of Technology, Azadi Ave, Tehran, Iran

P A P E R I N F O

Paper history:
Received 18 September 2023
Received in revised form 26 September 2023
Accepted 27 September 2023

Keywords:
DCB solder joint
Fracture energy
Random forest model
Lasso regression
NSGA-II algorithm

A B S T R A C T

Predicting the exact values of fracture load and energy has a significant effect in preventing solder joint failure. In this research, various double cantilever beam (DCB) solder joints with different geometric constraints, including adherend thickness, adherend width, loading arm length, and solder thickness were tested under mode I crack propagation and at a strain rate of 0.03 s^{-1}. According to ANOVA test results, all the mentioned geometric factors influence the fracture load, but adherend width and solder thickness don't change the failure energy remarkably, considering the type I error is equal to 0.05. The failure load and energy forecasting using the random forest algorithm showed that the prediction accuracy is 92% and 81% respectively. Linear regression and lasso regression were also utilized to identify the solder joint's fracture behavior. The coefficient of determination in both methods is acceptable for solder joint fracture force prediction, but for fracture energy, it has decreased to about 70%. Finally, multi-objective optimization was done with the help of the NSGA-II method, and the Pareto front diagram drawn according to the problem's constraints to find the optimal values for fracture force and energy.

doi:

1. INTRODUCTION

The vast advancement of technology in the field of electronics has led to the widespread use of Printed Circuit Boards (PCBs) to manufacture cutting-edge components. Therefore, these parts experience extensive loading conditions [1, 2]. In a general classification, the applied forces on solder joints can be divided into three categories. Thermal cycling loading, random vibration, and mechanical loading are among the most important types of loading conditions on solder joints [3]. Several factors, such as temperature changes, impact, and high ambient humidity can change the solder joint's optimal performance significantly. Because the most vital issue in the reliable performance of electronic parts is the solder joint and the inability reason for correct execution in many printed circuit boards comes from the joint fracture [4], much research has been done to investigate the solder joint performance in electronic devices. From the point of view of the mechanical loading on solder joints, applying quasi-static loading is one of the most vulnerable factors in their failure, which can cause bending or torsion in disparate section of the connection and leads to crack initiation [5]. With the growth of the initiated crack, failure of the solder joint occurs after some time. It is feasible to predict the fracture phenomenon in the solder joints by doing numerous experiments in different working conditions. It is astonishing how performing numerous experiments requires financial resources and spending a lot of time. Furthermore, because of the interaction between factors that influence solder joint fracture behavior, data collection must be done in full factorial mode to estimate the correlation between parameters [6]. This will increase the number of required experiments remarkably. In some research, statistical approaches have been utilized to predict solder joint reliability. For example, Weibull distribution has been employed to forecast solder joint reliability [7]. By calculating Weibull equation parameters according to finite element analysis results, a probability density diagram is drawn according to experiment sample results. In some cases, there are considerable differences between experimental and finite element simulation results. So, these methods can't predict solder joint degradation as well as required.

There are many variables, such as solder thickness, solder length, ambient humidity, and cooling rate, which can alter the fracture behavior in the solder joints [8]. In a predominantly categorizing, effective parameters in solder joints fracture load and energy can be split into three main groups: geometric constraints, manufacturing process, and loading mode situation. Nadimpali and Spelt [5], estimated the fracture load and energy in double cantilever beams

*Corresponding Author Email: nourani@sharif.edu (Amir Nourani)

(DCB) when they were subjected to mode I crack propagation loading condition. By changing geometrical factors, including the loading arm length and solder joint length, fracture load has been obtained for different conditions. According to the results, in DCB solder joints with less than 2.5 mm solder, failure occurs immediately after crack formation, while in samples with joint lengths more than 5 mm, failure occurs sometime after crack initiation because of R-curve toughening. Environmental working condition is another influential aspect of solder joint fracture demeanor. Examining the DCB specimens in the first mode of crack propagation and at a strain rate of 0.03 s^{-1}, revealed that increasing maintenance temperature and ambient humidity can decline the fracture load by an average of 33% and 15%, respectively. Fracture energy was also reduced because of the mentioned environmental changes significantly [9]. Different manufacturing processes can change the solder joint mechanical behavior by changing the mechanical properties. In [10], by testing DCB solder joint samples made of SAC713 at the constant strain rate of 0.5 s^{-1}, the effect of soldering temperature and time above liquidus (TAL) has been studied on the joint fracture load and critical strain energy release rate. According to the obtained results, increasing TAL from 1 minute to 2 minutes decreased the degradation load and energy, but soldering temperature had no effect on the failure load and energy. Additionally, rising the cooling rate has reduced the fracture force and energy as a consequence of IMC layer thickness reduction and alteration of the Cu_6Sn_5 and Ag_3Sn particles in the solder layer microstructure [11-13]. Geometric factors can also be important in solder joint fracture behavior. Increasing adherend thickness, which reduces the plastic zone area in DCB solder joints, caused a sharp increase in the sample's fracture load tested at mode I crack propagation. Critical strain energy release rate (J_{ci}) has also experienced a 70% reduction by changing adherend thickness from its minimum value to maximum [14]. Karimi and Nourani [15], prepared single lap shear (SLS) samples and evaluated the effect of geometrical factors like adherend thickness and solder length on fracture load and energy at the strain rate of 0.01 s^{-1}. They measured the energy dissipation using a 2-D cohesive zone modeling (CZM). According to outcome results, adherend thickness could make severe changes in fracture load values. Moreover, it has been shown that using dissimilar adherend thickness and solder length for making experimental specimens changes the plastic zone area and stress distribution in the solder material. Among the key components acting on solder joint fracture, loading condition is one of the deciding parameters. Solder joints can be subjected to axial, shear, or a combination of axial and shear loading. Different DCB samples made of SAC305 solder were examined in different loading mode ratios [16]. Mode ratio represents the ratio of axial to shear force applied to the solder joint according to the stress intensity factor in mode I and II crack propagation. with an increase in the loading mode ratio, which means raising the shear load applied to the solder joint, critical strain energy release rate is increased, and the required force for joint failure decreased. Nourani and Spelt [17], have studied the effect of loading speed (strain rate) and loading condition on characteristics of solder joints fracture. Fracture energy is significantly reduced by increasing the strain rate from a medium level (about 0.3 s^{-1}) to a high level (about 40 s^{-1}). For instance, when the loading phase angle is equal to 38 degrees and at a 30 s^{-1} strain rate, the J-integral value at the moment of crack formation is about 1000 J/m^2, but raising the strain rate to 60 s^{-1} caused a 50% reduction in critical strain energy release rate. The basis for the difference in the critical strain energy release rate at disparate strain rates is creep [18]. When the applied strain rate, for example, is of a quasi-static type, creep is also involved in crack growth. According to this fact, samples tested at quasi-static strain rate had lower fracture load and energy. Joint length also plays a crucial role in the fracture behavior of solder joints. Increasing solder joint length in double cantilever beam samples under bending revealed that increasing solder joint length up to about 30 mm, increases the breaking force noticeably [19].

Due to the worldwide use of artificial intelligence in recent years in various areas of science, researchers in the field of solder joints have also benefited from this issue, and a large number of research has been done regarding the application of machine learning in the field of solder joints [20-24]. Samavatian [25], identified important factors in printed circuit board failure caused by thermal cycling. They trained an artificial neural network which can predict the lifetime for desired solder joints in electronic components with 82% accuracy. Chen et al. [20] tried to estimate solder joint lifetime in a PCB with ball gay array configuration by means of neural networks. They considered 14 parameters influencing the lifetime of the solder joints as the network input vector and could predict the lifetime with 89% accuracy by using 360 data points. Neural network hyperparameter optimization was done to predict solder joint's mechanical behavior by considering barrel and hourglass shapes for joints. Different numbers of internal hidden layers and neurons in each hidden layer were the objective function for the optimization problem. According to outcome results, when the number of hidden layers and the number of neurons in each layer are equal to 3 and 50, respectively, the optimal point has been obtained in terms of accuracy and running time for the mentioned neural network. Another primary variable in specifying the reliable performance of solder joints is the random vibrations [26, 27]. In addition, location of different components on a PCB and soldering material are also among the principal parameters for determining solder joints fracture time. A multi-layer perceptron model was trained to forecast ball grid array solder joint life in a PCB by considering the mentioned parameters. To examine random vibration phenomena acting on the solder service lifetime, vibrations in different directions and angles are applied to printed circuit boards using finite element analysis. By training the desired neural network, the useful lifetime of the solder joints has been calculated with 91% accuracy [28].

According to the literature review, no research has been done about failure load and energy prediction in solder joints, especially when they are under mechanical loading.

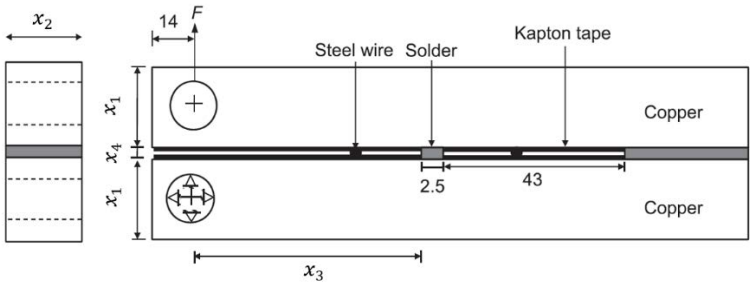

Figure 1. Two-dimensional image of double cantilever beam sample

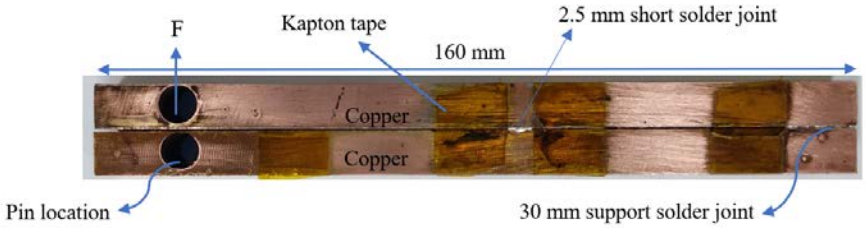

Figure 2. Side view of the prepared sample. Specimen depth is 10 mm

Therefore, in this research, various double cantilever beam samples have been tested to predict fracture load and critical strain energy release rate as the fracture energy of SAC305 solder joints. In the first step, effective geometric parameters that affect solder joint fracture behavior were identified with the help of the ANOVA test. Then, with the contribution of different machine learning methods, including random forest and regression, the solder joint's fracture load and energy were estimated. In the last section, fracture load and energy multi-objective optimization was done by using the NSGA-II algorithm.

2. EXPERIMENTAL APPROACH

In this section, laboratory sample preparation and fracture testing for double cantilever beam (DCB) solder joints by using a testing machine will be discussed.

2. 1. SPECIMEN EXPLANATION and PREPARATION

Double cantilever beams were made according to the surface mount technology (SMT) method. These samples can simulate the solder joint behavior on electronic boards [29, 30]. Copper rods made of C110 alloy have reached the dimension discussed in Figure 1. With the help of an ultrafine carbide/nylon polishing pad, scratches caused by the production process were removed. The copper bar surfaces were then placed in an ultrasonic cleaner to remove the residual impurities. After that, copper bars are removed from the ultrasonic cleaner and dried with a piece of cotton cloth. Soldering locations were cleaned with acetone to reach a better connection between solder and copper. A part of the sterile gauze pad was used to clean dirt from the surfaces. Then, solder fragments with different thicknesses were placed between copper bars and put down on the hot plate.

The soldering process done at a constant temperature of 220 ℃. Flux-cored Sn3.0Ag0.5Cu (SAC305) melting temperature occurs at this temperature [14]. For controlling the soldering length region, Kapton tape was used between two spaces that must be soldered. The sample is held on the hot plate between 1 minute to 2 minutes as TAL, after the solder joint melting happens. After that, the samples were cooled at a constant cooling rate of 1.4 $^{\circ C}/_{S}$, which is typical in microelectronic manufacturing [17, 31]. Finally, holes with a diameter of 7 mm are made in copper bars to fix the specimen in the fixture. Figure 2 illustrates a prepared DCB solder joint.

2. 2. FRACTURE TESTING

Fracture tests were done using a displacement-control situation under mode I loading condition using a hydraulic testing equipment, (Zwick-Roell Amsler-HCT 25-400). With the help of clearances made in copper bar holes, the initial movement of the testing machine actuator did not apply any load to the solder joint, and the sample was tested at a constant strain rate. The displacement actuator was tuned to produce the strain rate of 0.03 s^{-1} for all the experimental samples. The position of the specimen in the fixture is illustrated in Figure 3.

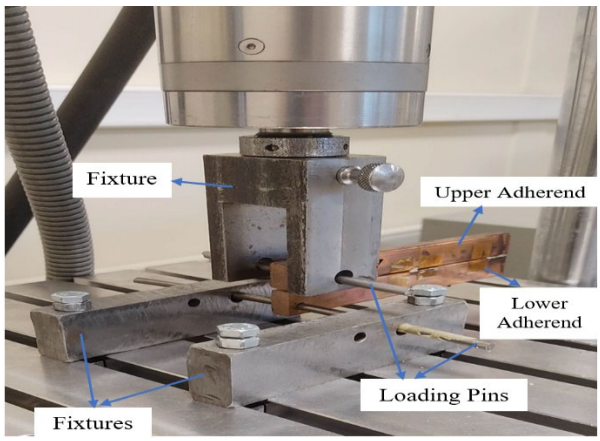

Figure 3. Description of DCB sample position in the fixture

The actuator cross-head speed calculation will be explained in the strain rate calculation section. Since the R-curve toughening is not seen in joints with less than 5mm in length, the maximum force applied to the solder joint was considered as failure load, which happened before a sudden eruption in the load cell output. The load-time diagram is depicted in Figure 4 to access the fracture load.

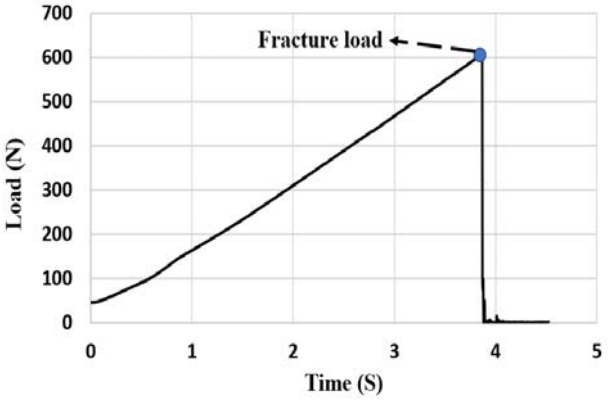

Figure 4. A typical Load-Time curve for DCB samples

3. FINITE ELEMENT MODELING

A comparison between the two-dimensional and three-dimensional models in [29] showed that a two-dimensional model can accurately estimate the fracture energy. In this study, the copper bars were simulated using plane-stress elements and the solder layer was modeled by plane-strain elements.

3. 1. STRAIN RATE CALCULATION

For all simulations, the mesh size varied from 0.05 mm in the solder layer to 1 mm in copper rods in line with [15] in order to achieve the exact value for the element's displacement. Strain rate calculation is based on the strain created at the crack initiation location in the solder joint. As described in Figure 1, the lower pin location was fixed, and a velocity equal to 1 mm/s was applied to the upper pin location in the finite element simulation. For strain calculation at the crack initiation location, the upper node (UN) and lower node (LN) vertical displacement have been calculated. Then, the strain is determined using the following equations [14]:

$$\varepsilon_y = \frac{UN - LN}{Solder\ Thickness} \quad (1)$$

Cross-head speed calculation at any desired strain rate has been calculated using Equation 2:

$$Strain\ rate = Cross - head\ speed \times \varepsilon_y \quad (2)$$

In Equation 2, the cross-head speed is in millimeters per second. The details of the finite element model used to calculate the strain rate are shown in Figure 5. SAC305 solder and copper bars properties used in the finite element models are listed in Table 1 [32, 33].

3. 2. FRACTURE ENERGY MEASUREMENT

The measured fracture load in the experiment for each sample was applied as input in the finite element model (FEM) to calculate the critical strain energy release rate as the main parameter in fracture energy. This method has been used widely for simulating the fracture behavior in layered ductile materials [34, 35].

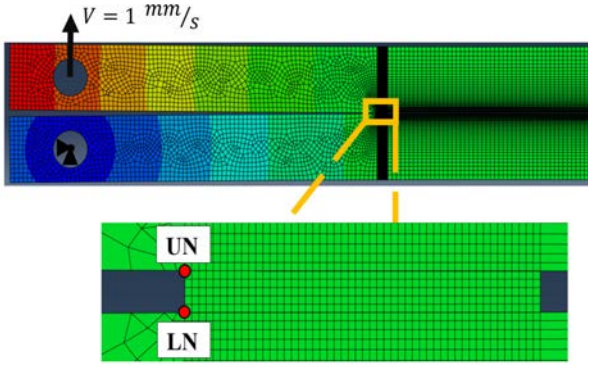

Figure 5. Finite element model for strain rate calculation

A load-geometry method was applied to compute the J_{ci}, using an elastic-perfectly plastic model for the solder. A pre-crack of 0.25 mm length was considered in the solder layer to be consistent with the approach used in [5, 8]. J-integral values obtained from the average of 4 contours surrounding the end of the crack [36].

TABLE 1. Solder and copper properties in the FEM model

Material	Young modulus (MPa)	Poisson ratio	Yield strength (MPa)
SAC305	51400	0.4	58
Copper C110	124000	0.35	-

4. RESULTS and DISCUSSION

Four geometric parameters were considered in this study. Adherend thickness (x_1), adherend width (x_2), loading arm length (x_3), and solder thickness (x_4) are these parameters. All of them are shown in Figure (1). The fracture force, F_{ci}, has been obtained for 80 fabricated laboratory samples at the constant strain rate of 0.03 s^{-1}.

4. 1. FUNCTIONAL PARAMETERS IDENTIFICATION

The effect of the considered factors was identified with the help of analysis of variance (ANOVA). To achieve this goal, five levels of change are examined for each of the investigated parameters (Table 2). The results of the ANOVA test performed on the experimental DCB solder joint samples are presented in Table 3. The effects of the four mentioned geometric constraints on the fracture load are listed in Table 3. By considering 95% reliability, all the variables had a meaningful impact on the sample's fracture load. Therefore, the initial assumption that indicates the equality of the average fracture force at different levels is rejected and there is a significant difference between the averages of dissimilar

levels. In accordance with the outcome results, loading arm length has the greatest effect on the solder joint's fracture load because of a larger F-value. Solder thickness has the least impression on the degradation force among the considered factors.

TABLE 2. Different levels of ANOVA test parameters

Parameter name	Level of changes value (mm)
Adherend thickness (x_1)	8 – 11 – 14 – 17 – 21
Adherend width (x_2)	8 – 11 – 14 – 17 – 21
Loading arm length (x_3)	12.7 – 25.4 – 38.1 – 48.2 – 71.1
Solder thickness (x_4)	0.15 – 0.25 – 0.45 – 0.5 – 1

The results of the ANOVA test to explore the geometric factors affecting the solder joint critical strain energy release rate, J_{ci}, which is considered as the fracture energy, are shown in Table 3. Loading arm length and adherend thickness are definitely important in estimating the fracture energy. Despite loading arm length and adherend thickness, adherend width and solder thickness have no meaningful upshot on fracture energy, considering 95% reliability. The P-value for adherend width is 0.07. This means that, with 93% certainty, the null hypothesis can be rejected. The null hypothesis expresses the equality of means at different levels. Therefore, if it is said that average fracture energy at different levels is not equal and the adherend thickness has a meaningful effect on critical strain energy release rate, this conclusion has 7% error. Similarly, if it is said that the solder thickness changes the specimen's fracture energy, this statement has a 35.3% error. So, adherend width and solder thickness can be ignored for fracture energy prediction, but we have considered them in different machine learning algorithms used for fracture energy prediction to attain a more accurate prediction.

TABLE 3. ANOVA test results for fracture load and energy

Parameter name	Fracture load test results		Fracture energy test results	
	F-value	P-value	F-value	P-value
Adherend thickness	67.19	0	16.04	0
Adherend width	33.18	0	3.06	0.07
Loading arm length	89.61	0	29.65	0
Solder thickness	11.7	0	1.24	0.353

In the ANOVA method, each data is divided into two components as follows [37]:

$$y_{ij} = \mu_i + \varepsilon_{ij} \quad (3)$$

y_{ij} is the j-th observation in the i-th level, μ_i is the mean of the i-th factor level and ε_{ij} is a random error part that incorporates all other sources of variability in the experiment. The described equation is also called the one-way or single-factor analysis of variance (ANOVA) model because only one factor is investigated. The decomposition of the variability in the observations through an ANOVA test is an algebraic relationship. However, the use of partitioning in the analysis of variance test requires that specific assumptions be satisfied. In practice, however, these assumptions will usually not hold exactly. Consequently, it is reasonable to rely on the results of the analysis of variance test when the validity of the considered assumptions has been checked. Violations of the basic assumptions and model adequacy can be investigated by examining residuals. We define the residual for observation j in treatment i as [37]:

$$e_{ij} = y_{ij} - \hat{y}_{ij} \quad (4)$$

$\hat{y}_{ij}$ indicates the fitted value for ij-th observation. In general, for checking the model adequacy, residuals must be structureless. On a closer look, the normal probability plot of residuals, residuals versus fitted plot and residuals versus observations order chart are drawn. These three plots are drawn for the solder thickness ANOVA fracture load test. Figure 6 presents the normal probability plot for residuals. If the underlying error distribution is normal, this plot will resemble a straight line and the adequacy of the model is confirmed.

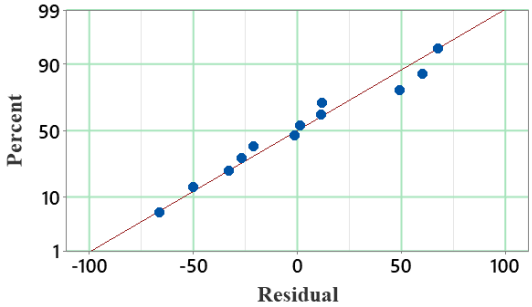

Figure 6. Normal probability plot for residuals

Therefore, standardized residuals must be checked. By sketching the residuals normal probability plot, outlier data can be identified by standardization of residuals. For this reason, standardized residual values obtained from Equation 4 must be tested:

$$d_{ij} = \frac{e_{ij}}{\sqrt{MS_E}} \quad (5)$$

MS_E is the mean-squared error [37]. For a suitable test, standardized residual values should fall within ± 3. If this happens, the normality assumption is correct. The highest value of standardized residuals for all ANOVA tests performed is equal to 2.38. Sequentially, the normality assumption is valid for all the situations. One of the other main aspects for checking the adequacy of the model is the constancy of different observations. If the changes are similar in the graph of the residuals versus fitted values, the variances are equal.

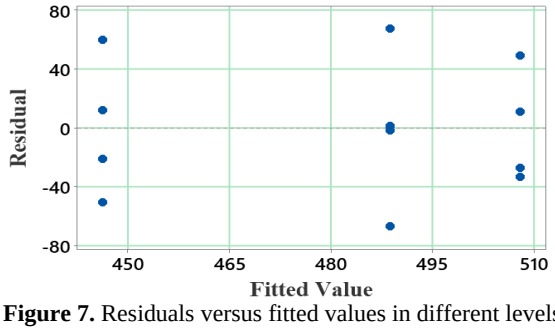

Figure 7. Residuals versus fitted values in different levels

Figure 7 specifies the residuals versus fitted values. As it is clear, residual value changes at different fitted levels are alike, and the same dispersion is observed at various stages of the fracture load.

Therefore, assuming equality of variances is right. The last thing that should be checked to assess the model adequacy is data independence. Figure 8 shows the residual changes according to observation order. If the changes in the residuals chart based on the observation order do not follow a special ascending or descending order for all the data, the samples have acceptable independence, as shown in Figure 8.

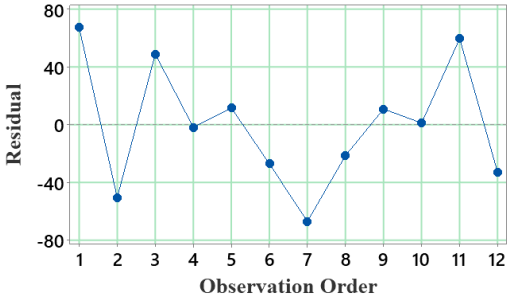

Figure 8. Data independence checking plot

Distance between the support solder and the main solder (2.5 mm length in Figure1) which is equal to 43 mm in Figure 1, is not among the main geometric parameters in DCB solder joints but, the possibility of the importance of this factor on the fracture load and energy has been investigated. 15 samples with different solders distance considered as 6.5, 23 and, 43 mm have been tested. Figure 9 indicates fracture load and energy as various solders distance. Increasing solder distance from 6.5 to 23 mm, caused a slight rise in fracture load and energy values. With further increase in solders distance from 23 to 43 mm, fracture load, F_{ci}, experienced a 63 N reduction and reached an average of 715 N, but fracture energy, J_{ci}, has remained constant with a perfect approximation and just increased about 7 $^{J}/_{m^2}$.

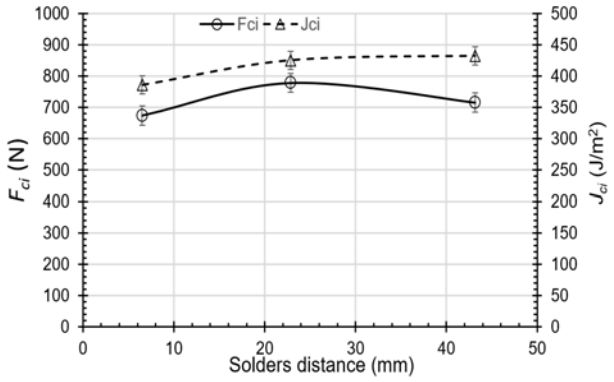

Figure 9. Fracture load and energy values at different solders distance levels

By performing an ANOVA test to conduct an investigation about the solders distance effect on fracture load and energy, by considering type I error equal to 0.05, the p-value parameter was equal to 0.17 and 0.328 for fracture load and energy, respectively. This means solders distance has no meaningful effect on solder joint failure load and energy, and can be ignored for reliability assessment in DCB solder joint prediction.

4. 2. RELIABILITY ASSESSMENT

In this section, an attempt was made to predict the fracture load and energy in DCB solder joints under mechanical loading with the help of the Random Forest algorithm. Additionally, linear and lasso regression methods employed to predict the failure force and critical strain energy release rate considering different geometric parameters.

Random forest is a kind of ensemble learning method that consists of a large number of Decision trees. Each decision tree predicts a value or specific class for the input data. Figure 10 shows the schematic of the random forest algorithm performance consisting of some decision trees. The final value or class for the desired data is calculated by averaging the output values of each decision tree for regression problems and the majority vote for classification problems. A decision tree is a recursive graph that can be used for decision-making. In each branching node of the decision tree, a specific feature is examined to split the dataset into different groups. To determine the goodness of an attribute for use at nodes, we need to compare the degree of the impurity of the parent node with the child nodes by using the Shannon entropy equation [38]:

$$Entropy\ (S) = \sum_{i=1}^{c} -p_i \log_2 p_i \tag{6}$$

p_i represents the probability of obtaining the $i-th$ event in all possible events, which shows with c. Then, by using information gain, which is based on the decrease in entropy after a dataset is split on an attribute, this process continues until all the data is sorted.

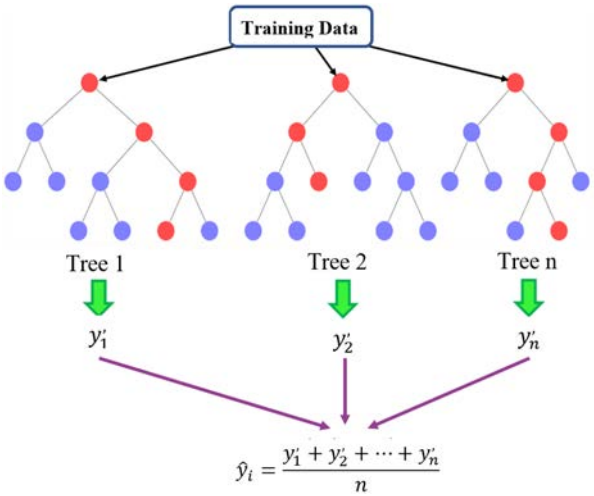

Figure 10. Schematic function of random forest model

80 data obtained from experiments is used for training and testing the random forest model. Due to the lack of much available data, only 10% of the dataset was used for testing the desired model. The applicable random forest model is designed in a way that provides the best results with the least amount of time spent on running. One of the important advantages of the random forest algorithm is the smaller number of unknown parameters that need to be adjusted by

training the model [39]. For example, unlike neural network models where weights between neurons, bias values and many other variables should be tuned in the training process, the random forest model has fewer unknown parameters. So, using random forest models can lead to more accurate results when a large dataset is unavailable. Figure 11 indicates the random forest predicted values versus measured values for solder joint fracture load.

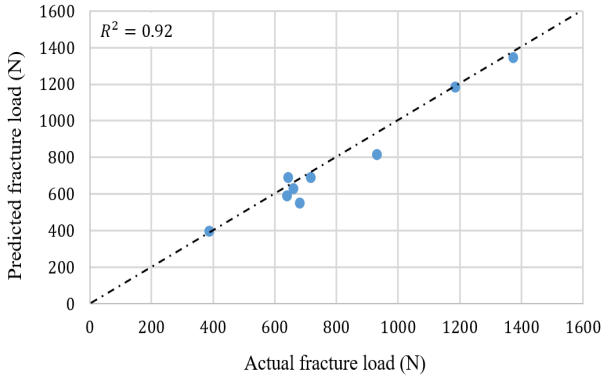

Figure 11. Random forest predicted values versus measured values for fracture load testing dataset

By training the desired algorithm on the data, the coefficient of determination (R^2) equals to 0.93 and 0.92 for training and testing datasets, respectively for DCB solder joint fracture load. This means that the designed model can predict the failure load with reasonable accuracy. Like what is described for fracture load forecasting, another random forest is used to predict the solder joints' critical strain energy release rate, J_{ci}, which is considered as fracture energy. The coefficient of determination in the random forest model, designed to predict the fracture energy, is equal to 0.838, for the training dataset and 0.81 for the testing dataset. One of the most vital parameters in random forest models is the number of decision trees in a random forest algorithm, which is known as n-estimators. This factor can influence prediction accuracy significantly. for this reason, it has been tried to reduce the prediction error of the random forest model by finding the optimal value for this hyperparameter (Figures 12 and 13).

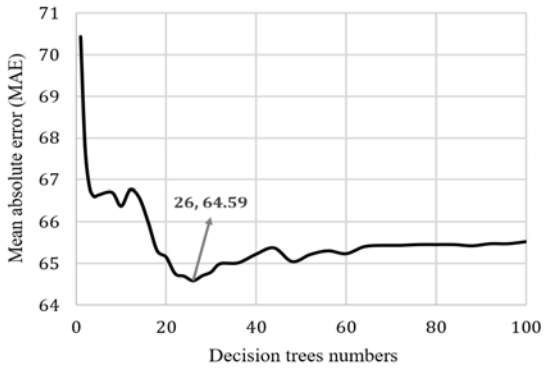

Figure 12. Random forest MAE in terms of decision tree numbers for fracture load prediction

The forecasting correctness of the desired model is measured using the mean absolute error (MAE):

$$MAE = \frac{\sum_{i=1}^{n}(\hat{y}_i - y_i)}{n} \quad (7)$$

The $\hat{y}_i$, y_i and n are respectively the predicted output, actual output and number of data points. By changing the number of decision trees, the effect of this parameter on MAE studied for fracture load and energy predictor models. Figure 12 and 13 illustrate the MAE for the training dataset for both models according to decision tree numbers.

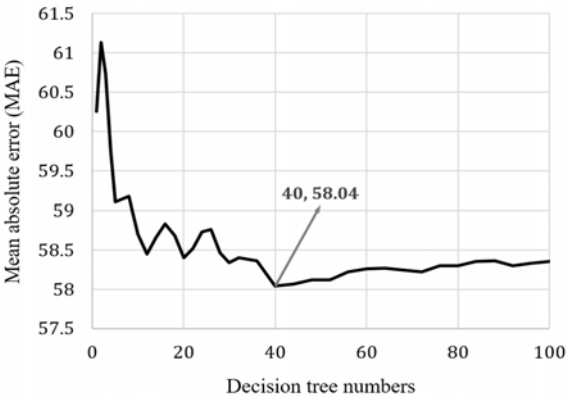

Figure 13. Random forest MAE in terms of decision tree numbers for fracture energy prediction

Lasso regression is a technique used on regression models in order to predict the desired output with more accuracy. Additionally, it can be used to perform a feature selection when there are a greater number of features available. This algorithm uses a shrinkage method to shrink data values towards a central point close to the means. It is a L1 regularization method. This means, a regularization term that penalizes large weights is added to the loss function as follows:

$$L_{reg}(\theta) = L(\theta) + \lambda \sum_{k} |\theta_k| \quad (8)$$

θ_k represents the weights, $L(\theta)$ is data loss and $\lambda \sum_k |\theta_k|$ shows regularization loss [40]. For every weight in the algorithm, we add a regularization term to the loss function. By means of this, every weight is decayed linearly toward zero during the gradient descent parameter update. The weight decay coefficient, which is represented by lambda (λ), determines the domination of regularization loss during the gradient computation. In this study, fracture load and energy were estimated using linear regression and lasso regression. 80 data were used for training and testing the model. 80% of the data have been used for training the model and the remaining 20% for testing the model. Table 4 reports the coefficient of determination for linear and lasso regression models for solder joints fracture load and energy prediction, considering the training and testing dataset. The difference between prediction accuracy on training data for fracture load and energy in linear regression and lasso regression methods is negligible. considering the test dataset for solder joint failure load and energy prediction, the contrast between these two methods is more noticeable. The lasso regression algorithm estimates the fracture load and energy for the testing dataset nearly 7% better. By increasing the dataset, the difference in prediction accuracy becomes clearer. This happens because of data

dispersion. The dispersion of data increases with the increase of their numbers. Therefore, data shrinkage can be more important.

TABLE 4. R-squared score for regression models

Data type \ Model	Linear regression	Lasso regression
Fracture load (Traning data)	0.915	0.932
Fracture load (Testing data)	0.82	0.8837
Fracture energy (Training data)	0.73	0.735
Fracture energy (Testing data)	0.64	0.71

According to Table 4, both lasso and linear regressor models cannot predict the solder joint's critical strain energy release rate with acceptable accuracy. So, we have used other regression models for fracture energy forecasting in DCB solder joints. By examining different types of regression, an exponential function has been chosen for fracture energy estimation with the highest coefficient of determination value which is illustrated in Equation 10.

One of the remarkable parameters in optimal performance of the lasso regression algorithm i the lambda (λ) value. This parameter can affect the prediction accuracy by changing the regularization loss as described in Equation 8. Actually, altering the lambda value can change the effect of regularization loss on data loss. By increasing the lambda value from 0.01 to 1, the effect of this parameter on the coefficient of determination (R^2) dataset for both fracture load and energy was studied. As Figure 14 shows, by increasing the lambda value from 0 to 0.53, the coefficient of determination has increased very slightly for the fracture load algorithm predictor. But further rise in lambda, caused the coefficient of determination to decline. The slight change in prediction accuracy is due to the limited dataset. The effect of lambda values on the fracture energy in lasso regression model has also been investigated. By enlarging the lambda value from 0 to 0.024, the coefficient of determination has been increased from 0.697 to 0.71 for testing data linearly. But after that, it decreased to 0.7 when the lambda value was equal to 1. Therefore, lambda values cannot change the model performance significantly.

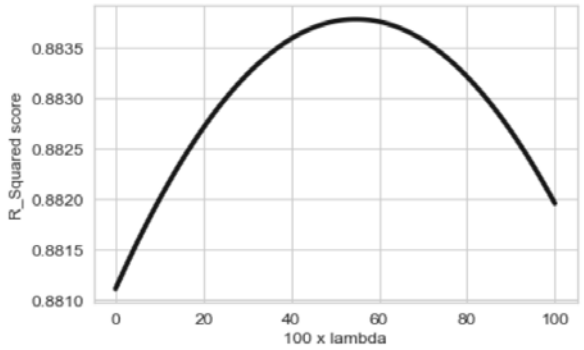

Figure 14. R-squared score versus different lambda values

4. 3. MULTIOBJECTIVE OPTIMIZATION

Achieving the optimal values for the solder joint fracture load and energy can have a notable effect on its reliable performance. According to this fact, we have tried to optimize the failure load and energy in DCB solder joints using equations obtained from regression algorithms for fracture load, F_{ci}, and energy, J_{ci}. The established equations for predicting fracture load and energy are as follows:

$$F_{ci} = 53.51x_1 + 52.05x_2 - 14.24x_3 + 381.85x_4 \quad (9)$$

$$ln\, J_{ci} = 6.59 - 0.094x_1 + 0.008x_2 + 0.01x_3 + 0.13x_4 \quad (10)$$

According to experimental samples, the constraints for variable designs are:

$$8 \le x_1 \le 21 \ mm \quad (11)$$

$$8 \le x_2 \le 21 \ mm \quad (12)$$

$$12.54 \le x_3 \le 71.12 \ mm \quad (13)$$

$$0.15 \le x_4 \le 0.45 \ mm \quad (14)$$

Fracture load and energy optimization was done with the help of NSGA-II algorithm. Figure 15 shows the multi-objective optimization Pareto front by considering Equations 9 and 10 as objective functions and Equations 11 to 14 for constraints.

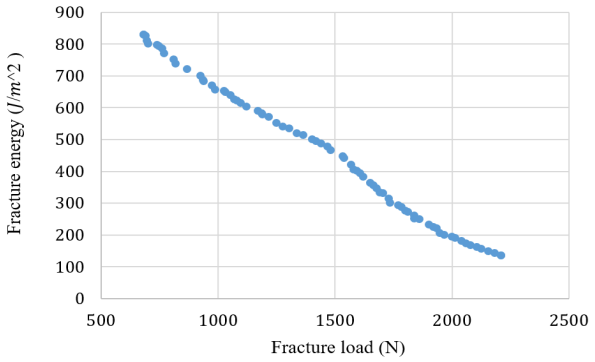

Figure 15. Pareto front diagram of the optimized problem

According to the drawn Pareto front, increasing the fracture load caused the decline in fracture energy values. Therefore, fracture load and fracture energy behave opposite to each other. Simultaneous maximization of failure load and energy is not possible. Table 5 shows the best answers according to desired Pareto front for failure load and fracture energy.

TABLE 5. Optimal values for fracture load and energy

x_1	x_2	x_3	x_4	F_{ci} (N)	J_{ci} (J/m^2)
11.94	20.81	14.37	0.41	1680	341
8.05	20.93	71.03	0.44	680	871
16.73	21	12.66	0.44	1929	214
8	20.86	54.24	0.42	911	732

5. CONCLUSIONS

Fracture tests on DCB solder joints considering adherend thickness, adherend width, loading arm length, and solder thickness as geometric constraints showed that all the four mentioned parameters affect the fracture load using a 95% confidence interval. Fracture energy, J_{ci}, was not a strong function of Adherend width and solder thickness according to the analysis of variance (ANOVA) test results.

Solder joint fracture load and energy prediction are done with the help of different machine learning algorithms. The random forest model estimated the failure force and energy for the test data with an accuracy of 92% and 81%, respectively. Also, the number of decision trees in the desired random forest algorithm was optimized as one of the critical hyperparameters in this model to achieve the lowest mean absolute error. Additionally, by using linear regression and lasso regression, fracture load and critical strain energy release rate were calculated for DCB solder joints with different geometric constraints. Both models forecasted the fracture load with an average accuracy of 85% and fracture energy with 67.5% accuracy. Due to the low coefficient of determination for fracture energy prediction, an exponential function was applied for this purpose. By using the functions obtained in the regression models, multi-objective optimization for failure load and energy was done with the help of the NSGA-II algorithm.

6. REFERENCES

[1] P. Yang, D. Liu, Y. Zhao, Y. Tang, and H. Wang, "Approach on the life-prediction of solder joint for electronic packaging under combined loading," *IEEE Transactions on Reliability*, vol. 62, no. 4, pp. 870-875, 2013, doi: https://doi.org/10.1109/TR.2013.2285038.

[2] P. Wang, Y. Lee, C. Lee, H. Chang, and K. Chiang, "Solder joint reliability assessment and pad size studies of FO-WLP with glass substrate," *IEEE Transactions on Device and Materials Reliability*, vol. 21, no. 1, pp. 96-101, 2021, doi: https://doi.org/10.1109/TDMR.2021.3056054.

[3] B. Qiu *et al.*, "Survey on Fatigue Life Prediction of BGA Solder Joints," *Electronics*, vol. 11, no. 4, p. 542, 2022, doi: https://doi.org/10.3390/electronics11040542.

[4] V. Samavatian, H. Iman-Eini, Y. Avenas, and M. Samavatian, "Effects of creep failure mechanisms on thermomechanical reliability of solder joints in power semiconductors," *IEEE Transactions on Power Electronics*, vol. 35, no. 9, pp. 8956-8964, 2020, doi: https://doi.org/10.1109/TPEL.2020.2973312.

[5] S. P. Nadimpalli and J. K. Spelt, "Fracture load prediction of lead-free solder joints," *Engineering Fracture Mechanics*, vol. 77, no. 17, pp. 3446-3461, 2010, doi: https://doi.org/10.1016/j.engfracmech.2010.09.012.

[6] S. Honarvar, A. Nourani, and M. Karimi, "Effect of thermal treatment on fracture behavior of solder joints at various strain rates: Comparison of cyclic and constant temperature," *Engineering Failure Analysis*, vol. 128, p. 105636, 2021, doi: https://doi.org/10.1016/j.engfailanal.2021.105636.

[7] S. Zhang, H. Zhao, H. Xu, and X. Fu, "Accelerative reliability tests for Sn3. 0Ag0. 5Cu solder joints under thermal cycling coupling with current stressing," *Microelectronics Reliability*, vol. 120, p. 114094, 2021, doi: https://doi.org/10.1016/j.microrel.2021.114094.

[8] A. Nourani and J. K. Spelt, "Effect of processing parameters on fracture toughness of lead-free solder joints," *Engineering Fracture Mechanics*, vol. 142, pp. 64-78, 2015, doi: https://doi.org/10.1016/j.engfracmech.2015.05.042.

[9] S. Honarvar, A. Nourani, and M. Karimi, "Effect of environmental conditions on fracture behavior of solder joints," *Theoretical and Applied Fracture Mechanics*, vol. 112, p. 102897, 2021, doi: https://doi.org/10.1016/j.tafmec.2021.102897.

[10] M. Mohammadiamiri, A. Nourani, and G. H. Farrahi, "Main and interaction effects of manufacturing variables on microstructure and fracture of solder-copper connections," *Engineering Failure Analysis*, vol. 139, p. 106449, 2022, doi: https://doi.org/10.1016/j.engfailanal.2022.106449.

[11] N. Murad, S. R. Aisha, and M. Ishak, "Effects of cooling rates on microstructure, wettability and strength of Sn3. 8Ag0. 7Cu solder alloy," *Procedia engineering*, vol. 184, pp. 266-273, 2017, doi: https://doi.org/10.1016/j.proeng.2017.04.094.

[12] L. R. Garcia, W. R. Osório, and A. Garcia, "The effect of cooling rate on the dendritic spacing and morphology of Ag3Sn intermetallic particles of a SnAg solder alloy," *Materials & Design*, vol. 32, no. 5, pp. 3008-3012, 2011, doi: https://doi.org/10.1016/j.matdes.2010.12.046.

[13] L. Lehman *et al.*, "Growth of Sn and intermetallic compounds in Sn-Ag-Cu solder," *Journal of Electronic Materials*, vol. 33, pp. 1429-1439, 2004, doi: https://doi.org/10.1007/s11664-004-0083-0.

[14] A. Nourani, S. Mirmehdi, G. Farrahi, and F. Soroush, "Predicting fracture of solder joints with different constraint factors," *Fatigue & Fracture of Engineering Materials & Structures*, vol. 42, no. 2, pp. 425-438, 2019, doi: https://doi.org/10.1111/ffe.12920.

[15] M. Karimi, A. Nourani, and S. Honarvar, "Geometry influence on fracture behavior of lap-shear solder joints," *IEEE Transactions on Components, Packaging and Manufacturing Technology*, vol. 12, no. 1, pp. 80-88, 2021, doi: https://doi.org/10.1109/TCPMT.2021.3132197.

[16] S. P. Nadimpalli and J. K. Spelt, "Mixed-mode fracture load prediction in lead-free solder joints," *Engineering Fracture Mechanics*, vol. 78, no. 2, pp. 317-333, 2011, doi: https://doi.org/10.1016/j.engfracmech.2010.09.011.

[17] A. Nourani and J. K. Spelt, "Combined effect of strain-rate and mode-ratio on the fracture of lead-free solder joints," *Materials & Design*, vol. 85, pp. 115-126, 2015, doi: https://doi.org/10.1016/j.matdes.2015.06.134.

[18] J. Zhao, Y. Mutoh, Y. Miyashita, and S. Mannan, "Fatigue crack-growth behavior of Sn-Ag-Cu and Sn-Ag-Cu-Bi lead-free solders," *Journal of Electronic Materials*, vol. 31, pp. 879-886, 2002, doi: https://doi.org/10.1007/s11664-002-0199-z.

[19] S. Akbari, A. Nourani, and J. K. Spelt, "Effect of solder joint length on fracture under bending," *Journal of Electronic Materials*, vol. 45, pp. 473-485, 2016, doi: https://doi.org/10.1007/s11664-015-4133-6.

[20] T.-C. Chen, F. J. I. Alazzawi, A. A. Salameh, A. A. Ayub Ahmed, I. Pustokhina, A. Surendar, and A. Y. Oudah, "Application of machine learning in rapid analysis of solder joint geometry and type on thermomechanical useful lifetime of electronic components," *Mechanics of Advanced Materials and Structures*, vol. 30, no. 2, pp. 373-381, 2023, doi: https://doi.org/10.1080/15376494.2021.2014002.

[21] V. Voet, F. Van Loock, C. De Fruytier, A. Simar, and T. Pardoen, "Machine learning aided modelling of thermomechanical fatigue of solder joints in electronic component assemblies," *International Journal of Fatigue*, vol. 167, p. 107298, 2023, doi: https://doi.org/10.1016/j.ijfatigue.2022.107298.

[22] T.-C. Chen, M. J. C. Opulencia, H. S. Majdi, A. T. Hammid, H. Sharma, S. Sajjadifar, and A. Surendar, "Estimation of thermomechanical fatigue lifetime of ball grid solder joints in electronic devices using a machine learning approach," *Journal of Electronic Materials*, vol. 51, no. 7, pp. 3495-3503, 2022, doi: https://doi.org/10.1007/s11664-022-09635-2.

[23] S. Muench, D. Bhat, L. Heindel, P. Hantschke, M. Roellig, and M. Kaestner, "Performance assessment of different machine learning algorithm for life-time prediction of solder joints based

on synthetic data," in *2022 23rd International Conference on Thermal, Mechanical and Multi-Physics Simulation and Experiments in Microelectronics and Microsystems (EuroSimE)*, 2022: IEEE, pp. 1-10, doi: https://doi.org/10.1109/EuroSimE54907.2022.9758919.

[24] C. C. Yuan and C.-C. Lee, "Solder joint reliability modeling by sequential artificial neural network for glass wafer level chip scale package," *IEEE Access*, vol. 8, pp. 143494-143501, 2020, doi: https://doi.org/10.1109/ACCESS.2020.3014156.

[25] V. Samavatian, M. Fotuhi-Firuzabad, M. Samavatian, P. Dehghanian, and F. Blaabjerg, "Correlation-driven machine learning for accelerated reliability assessment of solder joints in electronics," *Scientific reports*, vol. 10, no. 1, p. 14821, 2020, doi: https://doi.org/10.1038/s41598-020-71926-7.

[26] H. Qi, M. Osterman, and M. Pecht, "A rapid life-prediction approach for PBGA solder joints under combined thermal cycling and vibration loading conditions," *IEEE Transactions on Components and Packaging Technologies*, vol. 32, no. 2, pp. 283-292, 2009.

[27] P. Yang and Z. Chen, "Experimental approach and evaluation on dynamic reliability of PBGA assembly," *IEEE Transactions on Electron Devices*, vol. 56, no. 10, pp. 2243-2249, 2009, doi: https://doi.org/10.1109/TED.2009.2027974.

[28] A. A. Salameh, H. Hosseinalibeiki, and S. Sajjadifar, "Application of deep neural network in fatigue lifetime estimation of solder joint in electronic devices under vibration loading," *Welding in the World*, vol. 66, no. 10, pp. 2029-2040, 2022, doi: https://doi.org/10.1007/s40194-022-01349-7.

[29] A. Nourani, S. Akbari, and J. K. Spelt, "Comparison of solder joint fracture behavior in Arcan and DCB specimens," *Engineering Fracture Mechanics*, vol. 143, pp. 47-62, 2015, doi: https://doi.org/10.1016/j.engfracmech.2015.06.036.

[30] R. Berni, M. Catelani, C. Fiesoli, and V. L. Scarano, "A comparison of alloy-surface finish combinations considering different component package types and their impact on soldering reliability," *IEEE Transactions on Reliability*, vol. 65, no. 1, pp. 272-281, 2015, doi: https://doi.org/10.1109/TR.2015.2455973.

[31] S. P. Nadimpalli and J. K. Spelt, "R-curve behavior of Cu–Sn3. 0Ag0. 5Cu solder joints: Effect of mode ratio and microstructure," *Materials Science and Engineering: A*, vol. 527, no. 3, pp. 724-734, 2010, doi: https://doi.org/10.1016/j.msea.2009.08.046.

[32] H.-T. Lee, M.-H. Chen, H.-M. Jao, and T.-L. Liao, "Influence of interfacial intermetallic compound on fracture behavior of solder joints," *Materials Science and Engineering: A*, vol. 358, no. 1-2, pp. 134-141, 2003, doi: https://doi.org/10.1016/S0921-5093(03)00277-6.

[33] I.-D. You and H.-K. Kim, "Evaluation of the joint strength between Sn–3.0 Ag–0.5 Cu solders and Cu substrate at high strain rates," *Materials Science and Engineering: A*, vol. 556, pp. 551-557, 2012, doi: https://doi.org/10.1016/j.msea.2012.07.025.

[34] G. Fernlund, M. Papini, D. McCammond, and J. Spelt, "Fracture load predictions for adhesive joints," *Composites Science and Technology*, vol. 51, no. 4, pp. 587-600, 1994, doi: https://doi.org/10.1016/0266-3538(94)90091-4.

[35] P. Fraisse and F. Schmit, "Use of J-integral as fracture parameter in simplified analysis of bonded joints," *International Journal of fracture*, vol. 63, pp. 59-73, 1993, doi: https://doi.org/10.1007/BF00053316.

[36] J. R. Rice, "A path independent integral and the approximate analysis of strain concentration by notches and cracks," 1968, doi: https://doi.org/10.1115/1.3601206.

[37] D. C. Montgomery, *Design and analysis of experiments*. John wiley & sons, 2017.

[38] C. Palamidessi and M. Romanelli, "Feature selection in machine learning: R\'enyi min-entropy vs Shannon entropy," *arXiv preprint arXiv:2001.09654*, 2020, doi: https://doi.org/10.48550/arXiv.2001.09654.

[39] J. Prost, U. Cihak-Bayr, I. A. Neacşu, R. Grundtner, F. Pirker, and G. Vorlaufer, "Semi-supervised classification of the state of operation in self-lubricating journal bearings using a random forest classifier," *Lubricants*, vol. 9, no. 5, p. 50, 2021, doi: https://doi.org/10.3390/lubricants9050050.

[40] J. Heaton, "Ian Goodfellow, Yoshua Bengio, and Aaron Courville: Deep learning: The MIT Press, 2016, 800 pp, ISBN: 0262035618," *Genetic programming and evolvable machines*, vol. 19, no. 1-2, pp. 305-307, 2018.

6. APPENDIX

In this section, the dataset related to the different ANOVA tests is presented. The value of adherend thickness, adherend width, loading arm length and solder thickness are equal to 14, 14, 71.1 and 0.25 mm, respectively in tests where these variables did not change and had a constant value.

TABLE A1. Adherend thickness ANOVA test data

Data Number	$x_1\ (mm)$	$F_{ci}\ (N)$	$J_{ci}\ \left(J/m^2\right)$
1	8	405	1166
2	11	506	557
3	14	644	384
4	17	858	358
5	21	1170	368
6	8	390	1099
7	11	582	695
8	14	642	383
9	17	818	333
10	21	1108	336
11	8	309	749
12	11	580	880
13	14	716	458
14	17	823	336
15	21	976	271

TABLE A2. Adherend width ANOVA test data

Data Number	$x_2\ (mm)$	$F_{ci}\ (N)$	$J_{ci}\ \left(J/m^2\right)$
1	8	393	428
2	11	663	596
3	14	644	384
4	17	1008	578
5	21	1160	518
6	8	343	341
7	11	684	626
8	14	876	634
9	17	929	509
10	21	924	357
11	8	368	384
12	11	613	527
13	14	685	425
14	17	981	557
15	21	1043	472

TABLE A3. Loading arm length ANOVA test data

Data Number	$x_3\ (mm)$	$F_{ci}\ (N)$	$J_{ci}\ \left(J/m^2\right)$
1	12.7	1523	214
2	25.4	1367	352
3	38.1	1185	398.2
4	48.2	1060	509
5	71.1	644	384
6	12.7	1533	219
7	25.4	1374	354
8	38.1	1124	366
9	48.2	1003	465
10	71.1	642	383
11	12.7	1384	185
12	25.4	1344	342
13	38.1	1280	450
14	48.2	974	444
15	71.1	716	458

TABLE A4. Solder thickness ANOVA test data

Data Number	$x_4\ (mm)$	$F_{ci}\ (N)$	$J_{ci}\ \left(J/m^2\right)$
1	0.15	650	557
2	0.25	655	571
3	0.45	905	621
4	0.5	732	487
5	1	1004	634
6	0.15	615	481
7	0.25	716	525
8	0.45	823	601
9	0.5	650	422
10	1	947	384
11	0.15	590	473
12	0.25	685	490
13	0.45	682	576
14	0.5	617	557
15	1	879	571